SUPPORTING INFORMATION

Detection of 1H-Triphosphirene (*c*-HP_3) and 2-Triphosphenylidene (HP_3) – the Isovalent Counterparts of 1H-Triazirine (*c*-HN_3) and Hydrazoic Acid (HN_3)

Chaojiang Zhang,[a, b] *Cheng Zhu,*[a, b] *André K. Eckhardt,*[c]* *Ralf I. Kaiser*[a, b]*

[a] Department of Chemistry, University of Hawaii at Manoa, 2545 McCarthy Mall, Honolulu, HI 96822 (USA)

[b] W. M. Keck Laboratory in Astrochemistry, University of Hawaii at Manoa, 2545 McCarthy Mall, Honolulu, HI 96822 (USA)

[c] Lehrstuhl für Organische Chemie II, Ruhr-Universität Bochum, 44780 Bochum (Germany)

* Correspondence to: Andre.Eckhardt@rub.de; ralfk@hawaii.edu.

EXPERIMENTAL METHODS

The experiments were carried out in an ultra-high vacuum chamber (UHV) pumped to a base pressure of 7×10^{-11} Torr[1, 2] utilizing turbomolecular pumps (Osaka, TG1300MUCWB and TG420MCAB) backed with oil-free scroll pumps (Edwards GVSP30). Within the chamber, a fine polished silver wafer is mounted to a copper cold head cooled by a closed-cycle helium refrigerator (Sumitomo Heavy Industries, RDK−415E) capable of achieving temperatures to 5.0 ± 0.1 K. The wafer can be translated vertically and rotated in the horizontal plane with a linear translator (McAllister, BLT106) and rotational feedthrough (Thermionics Vacuum Products, RNN−600/FA/MCO), respectively. During the experiment, phosphine (PH_3, Sigma−Aldrich, 99.9995%) and dinitrogen (N_2, Matheson, 99.9992%) (or 15-dinitrogen ($^{15}N_2$, Sigma-Aldrich, 98% ^{15}N)) gases were co-deposited onto the silver wafer via two separate glass capillary arrays to produce ice mixtures of PH_3 and N_2 with a composition ratio of (1.2 ± 0.2) : 1. The ice thickness was determined via exploiting laser interferometry by monitoring the interference fringes of a 632.8 nm helium-neon laser (CVI Melles Griot, 25-LHP-230) that is reflected from the silver wafer (2° relative to the ice surface normal). With the refractive indexes of pure PH_3 and N_2 ices (n_{PH_3} = 1.51 ± 0.04, n_{N_2}= 1.21 ± 0.01) and their composition ratio (PH_3 : N_2 = (1.2 ± 0.2) : 1), the thickness of the ice mixtures was estimated to be 1000 ± 50 nm.

After the deposition, the ices were examined utilizing a Fourier transform infrared (FTIR) spectrometer (Nicolet 6700, 6000 – 400 cm^{-1}, 4 cm^{-1} spectral resolution). The ice composition was calculated using a modified Beer-Lambert law. For PH_3, based on the absorption coefficients for the 2319 cm^{-1} (ν_1/ν_1, 4.7×10^{-18} cm molecule^{-1}) and 983 cm^{-1} (ν_2, 5.1×10^{-19} cm molecule^{-1}) bands along with corresponding integrated areas, its average column density was determined to be $(1.5 \pm 0.3) \times 10^{18}$ molecules cm^{-2}, which can be converted to 550 ± 60 nm thick ice with the density

of PH_3 ice (0.9 g cm^{-3}). Considering the thickness of the total ice (1000 ± 50 nm) and PH_3 ice (550 ± 60 nm), the thickness of N_2 was estimated to be 450 ± 50 nm, which corresponds to a column density of (1.2 ± 0.3) × 10^{18} molecules cm^{-2} taking into account the densities of N_2 ice (0.94 ± 0.02 g cm^{-3}). Therefore, the ratio of PH_3 and N_2 was found to be (1.2 ± 0.2) : 1.

The ices were then isothermally processed by 5 keV electrons (Specs EQ 22–35 electron source) at 5.0 ± 0.1 K for 120 minutes at currents of 0 nA (blank) and 100 nA. The electron incidence angle is 70° to the ice surface normal. Utilizing Monte Carlo simulations (CASINO 2.42), the maximum and average depths of the electrons were estimated to be 880 ± 90 and 490 ± 50 nm, respectively, which are less than the ice thickness (1000 ± 50 nm) avoiding interaction between the electrons and the silver wafer (Table S1). The irradiation doses were determined to be 26 ± 4 eV per PH_3 molecule and 21 ± 3 eV per N_2 molecule. To monitor the evolution of the ices during the electron irradiation, *in situ* FTIR spectra were recorded at intervals of 2 min.

After the irradiation, the ices were annealed to 300 K at 1 K min^{-1} (temperature programmed desorption (TPD) exploiting a programmable temperature controller (Lakeshore 336). During the TPD phase, the subliming molecules from the ices were examined using a reflectron time-of-flight (ReTOF) mass spectrometer (Jordon TOF Products, Inc.) coupled with tunable vacuum ultraviolet (VUV) photon ionization (Table S2). Three photon energies of 10.49, 8.53 and 8.20 eV were selected to distinguish the P_3H distinct isomers. The 10.49 eV (118.222 nm) laser was generated via frequency tripling ($\omega_{vuv} = 3\omega_1$) of the third harmonic (355 nm) of the fundamental (1064 nm) of a Nd:YAG laser using xenon (Xe) as a non-linear medium. To produce 8.53 eV (145.351 nm) and 8.20 eV (151.200 nm) lights, the second harmonic (532 nm) of an Nd:YAG laser was used to pump a Rhodamine 610/640 dye mixture (0.17/0.04 g L^{-1} ethanol) to obtain 606.948 nm (2.04 eV) (Sirah, Cobra−Stretch), which underwent a frequency tripling process to achieve ω_1 = 202.316 nm

(6.13 eV) (β−BaB_2O_4 (BBO) crystals, 44° and 77°). A second Nd:YAG laser (second harmonic at 532 nm) pumped DCM dye (0.30 g L^{-1} dimethyl sulfoxide) and Rhodamine 610/640 dye mixture (0.17/0.04 g L^{-1} ethanol) to obtain ω_2 = 665 nm (1.86 eV) and ω_2 = 611 nm (2.03 eV), which underwent a frequency doubling process to achieve ω_2 = 332.5 nm (3.73 eV) and ω_2 = 305.5 nm (4.06 eV) (β−BaB_2O_4 (BBO) crystals, 44°) and then combined with $2\omega_1$ generating ω_{vuv} = 8.53 eV (145.351 nm) and 8.20 eV (151.200 nm) at 1012 photons per pulse via difference four-wave mixing ($\omega_{vuv} = 2\omega_1 - \omega_2$) in pulsed gas jets of krypton (Kr) (Table S2). The VUV photons were spatially separated from the incident lasers ($2\omega_1$ and ω_2) and other wavelengths generated via multiple resonant and non-resonant processes ($2\omega_1 + \omega_2$; $3\omega_1$; $3\omega_2$) utilizing a biconvex lens made with lithium fluoride (LiF) (ISP Optics) and directed 2 mm above the ice surface for ionizing the sublimed species. The ionized molecules were examined with the ReTOF mass spectrometer based on their arrival time to a multichannel plate (MCP), which is correlated with mass-to-charge ratios (m/z). The MCP signal was first amplified by a fast preamplifier (Ortec 9305) and then recorded using a multichannel scalar (MCS) (FAST ComTec, P7888−1 E). The MCS is triggered by a pulse generator (Quantum Composers 9518) at 30 Hz. Each final mass spectrum is the average of 3600 sweeps of the flight time in 4 ns bin width and correlates to 2 K increase of the sample temperature.

COMPUTATIONAL METHODS

All computations were carried out with Gaussian 16, Revision C.01[3]. For geometry optimizations and frequency computations, the density functional theory (DFT) B3LYP functional[4-6] was employed utilizing the Dunning correlation consistent split valence basis set cc-pVTZ.[7] Based on these geometries, the corresponding frozen-core coupled cluster[8-11] CCSD(T)/cc-pVDZ, CCSD(T)/cc-pVTZ, and CCSD(T)/cc-pVQZ single-point energies were computed and extrapolated to complete basis set limit[12] CCSD(T)/CBS with B3LYP/cc-pVTZ zero-point

vibrational energy (ZPVE) corrections. The adiabatic ionization energies (IEs) were computed by taking the ZPVE corrected energy difference between the neutral and ionic species that correspond to similar conformations. As in general the difference of heavier isotopologues and standard isotopologues in the zero-point vibrational energy is marginal we used the ZPVEs of standard isotopologues for IE calculation and assume them as the same for our experiments with heavier isotopologues. The electric field of the extractor plate of our experimental setup lowers the ionization energy by up to 0.03 eV. Errors of the IEs are determined to be −0.08 eV to + 0.07 eV through a comparison of experimentally known IEs with computational benchmarks (Table S3).

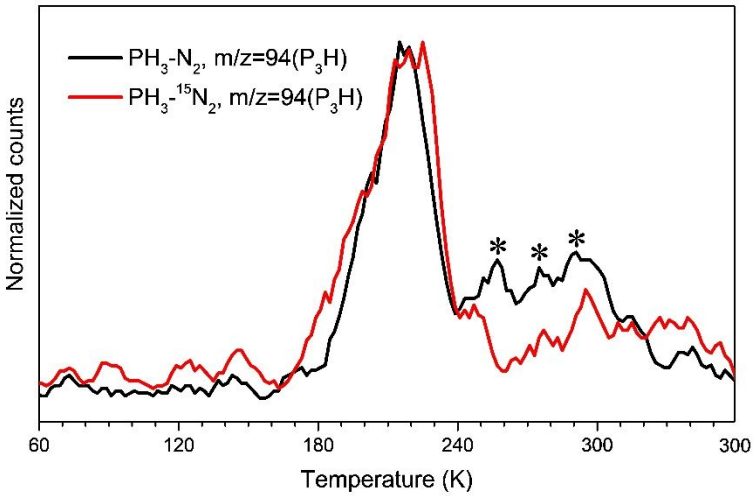

Figure S1. Temperature-programmed desorption (TPD) profile recorded at *m/z* = 94 from the electron processed phosphine (PH_3) – dinitrogen (N_2) and phosphine (PH_3) – 15-dinitrogen ($^{15}N_2$) ices via photoionization reflectron time-of-flight mass spectrometry (PI–ReTOF–MS) at a photon energy of 10.49 eV. The lack of any shift of the TPD profile at *m/z* = 94 in the temperature range from 175 K to 240 K reveals that the molecule of interest does not carry a nitrogen atom. The peaks marked with asterisk result from photo fragment ions from P_5H_3 (257 K) and P_5NH_2 (275 K, 291 K) (Figure S2).

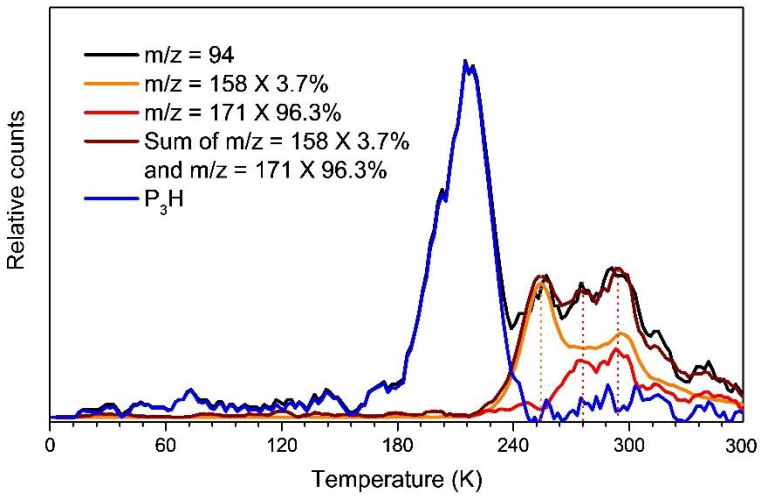

Figure S2. Temperature-programmed desorption (TPD) profile of HP_3 (blue line) at a photo energy of 10.49 eV. The signal at $m/z = 94$ in the temperature range from 175 K to 240 K originates from photo fragment ions from P_5H_3 (257 K; 158 amu) and P_5NH_2 (275 K, 291 K; 171 amu). By subtracting the photofragmentation signals, the TPD profile of HP_3 isomers at 10.49 eV was obtained and presented in Figure 3A (black line).

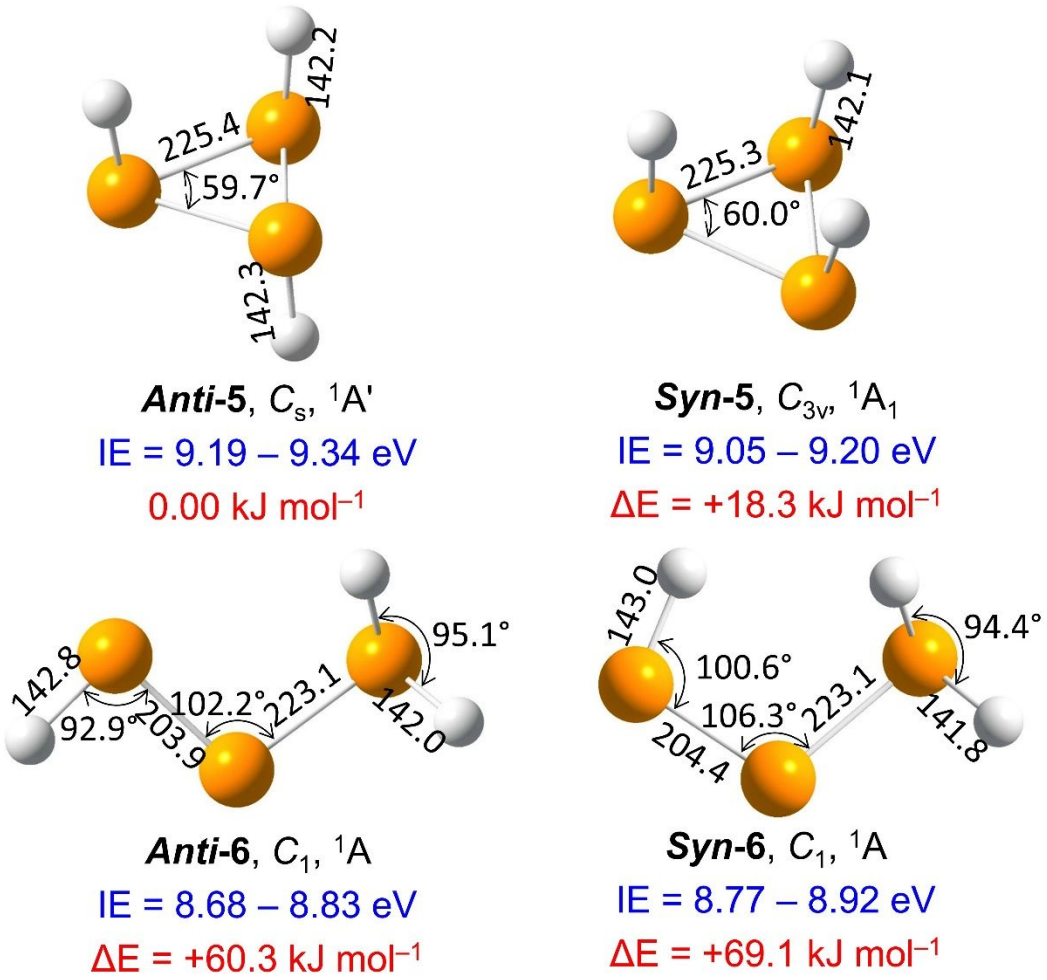

Figure S3. Molecular structures of P_3H_3 isomers. Bond lengths are given in picometers (pm) and bond angles in degree; point groups, electronic ground states, computed adiabatic ionization energies corrected for the electric field effect (blue), and relative energies (red) are also shown. The energies were computed at the CCSD(T)/CBS//B3LYP/cc-pVTZ plus zero-point vibrational energies level of theory. The atoms are color coded in white (hydrogen) and orange (phosphorous). Coordinates and normal modes are provided in Table S7.

Table S1. Data were used to calculate the average irradiation dose per molecule.

Initial kinetic energy of the electrons, E_{init} (keV)		5
Ice		$PH_3 + N_2$
Irradiation current, I (nA)		100 ± 5
Total number of electrons		$(4.5 \pm 0.5) \times 10^{15}$
Average penetration depth, l_{ave} (nm)[a]		490 ± 50
Maximum penetration depth, l_{max} (nm)[a]		880 ± 90
Average kinetic energy of backscattered electrons, E_{bs} (keV)[a]		2.96 ± 0.30
Fraction of backscattered electrons, f_{bs}[a]		0.12 ± 0.01
Average kinetic energy of transmitted electrons, E_{trans} (keV)[a]		0
Fraction of transmitted electrons, f_{trans}[a]		0
Irradiated area, A (cm^2)		1.0 ± 0.1
Dose (eV/molecule)	PH_3	26 ± 4
	N_2	21 ± 3

Note:

[a] Parameters obtained using the CASINO software v2.42.

Table S2. Parameters for the vacuum ultraviolet (VUV) light generation used in the present experiments.[a]

$2\omega_1 - \omega_2$	Photoionization energy (eV)	10.49 ($3\omega_1$)	8.53	8.20
	Flux (10^{11} photons s^{-1})	12 ± 1	10 ± 1	10 ± 1
	Wavelength (nm)	118.222	145.351	151.200
ω_1	Wavelength (nm)	355	202.316	202.316
Nd:YAG (YAG A)	Wavelength (nm)	355	532	532
Dye laser (DYE A)	Wavelength (nm)	-	606.948	606.948
Dye		-	Rhodamine 610 and 640	Rhodamine 610 and 640
ω_2	Wavelength (nm)	-	332.5	305.5
Nd:YAG (YAG B)	Wavelength (nm)	-	532	532
Dye laser (DYE B)	Wavelength (nm)	-	665	611
Dye		-	DCM	Rhodamine 610 and 640
	Nonlinear medium	Xe	Kr	Kr

Note:

[a] The uncertainty for VUV photon energies is 0.001 nm.

Table S3. Computed adiabatic ionization energies (IEs) of distinct HN_3 and HP_3 isomers along with error limits and previous computational (CCSD(T)/CBS//B3LYP/cc–pVTZ + zero-point vibrational energy (ZPVE) corrections) and experimental benchmarks of different nitrogen- and phosphorus-containing compounds. An offset of 0.03 eV was subtracted to correct for the electric field effect.

Compounds	Experimental IE (eV)	Experimental Error Limits (eV)	Computed IE (eV)	Computed IE–Experimental IE (max) (eV)	Computed IE–Experimental IE (min) (eV)	IE range after error analysis (eV)	Corrected IE with electric field effect (eV)
Ammonia NH_3	10.07 ± 0.02	10.05 – 10.09[1]	10.15	+0.06	+0.10		
Phosphine PH_3	9.869 ± 0.002	9.867 – 9.871[1]	9.82	–0.051	–0.047		
Hydrogen cyanide HCN	13.60 ± 0.01	13.59 – 13.61[1]	13.57	–0.04	–0.02		
Methinophosphide HCP	10.79 ± 0.01	10.78 – 10.80[2]	10.76	–0.04	–0.02		
Acetonitrile CH_3CN	12.20 ± 0.01	12.19 – 12.21[3]	12.20	–0.01	+0.01		
Methyl Isocyanide CH_3NC	11.24 ± 0.01	11.23 – 11.25[3]	11.25	+0.00	+0.02		
2H-Azirine c-H_2CCHN	10.05 ± 0.03	10.02 – 10.08[3]	10.02	–0.06	+0.00		
Hydrazoic acid HN_3 (**1**)			10.73			10.65 – 10.80 eV	10.62 – 10.77 eV
1H-triazirine HN_3 (**2**)			11.11			11.03 – 11.18 eV	11.00 – 11.15 eV
1H-triphosphirene HP_3 (**3**)			8.92			8.84 – 8.99 eV	8.81 – 8.96 eV
2-triphosphenylidene HP_3 (**4**)			8.44			8.36 – 8.51 eV	8.33 – 8.48 eV
				Average –0.04 ± 0.04	Average 0.02 ± 0.05		
				Error Limits –0.08 – +0.00	Error Limits –0.02 – +0.07		
				Combined Error Limits –0.08 – +0.07			

NOTE: 1. S. G. Lias, (2018).
2. D. C. Frost, S. T. Lee, C. A. McDowell, (1973).
3. A. M. Turner, S. Chandra, R. C. Fortenberry, R. I. Kaiser, (2021).

Table S4. Infrared absorption peaks before and after irradiation for phosphine (PH_3) – dinitrogen (N_2)/15-dinitrogen ($^{15}N_2$) ices.

Pristine ice, before irradiation (5 K)		
Assignment	Position with ^{14}N (cm^{-1})	Position with ^{15}N (cm^{-1})
PH_3 (ν_2)	983	982
PH_3 (ν_4)	1098	1098
PH_3 ($\nu_2 + \nu_4$)	2074, 2087	2075, 2089
PH_3 ($2\nu_4$)	2199	2200
PH_3 (ν_1/ν_3)	2314	2315
PH_3 ($\nu_1/\nu_3+\nu_L$)	2435	2435
PH_3 ($\nu_1+\nu_4$)	3398	3399
New peaks after irradiation (5 K)		
ν (P–N)	788	784
ν (PH_2)	1063	1063
ν (PH)	2270	2270

Table S5. Cartesian coordinates (distances in Å), vibrational frequencies (cm^{-1}), and intensity ($km\ mol^{-1}$) for selected structures of HN_3.

HN_3

1

H	1.894242	–0.503827	0.000000
N	0.945738	–0.872137	0.000000
N	0.125124	0.050764	0.000000
N	–0.733705	0.779359	0.000000

Frequency/ cm^{-1}	Intensity/ $km\ mol^{-1}$
549.9952	15.0399
620.1353	0.0185
1185.9459	217.9182
1303.2957	2.7823
2277.9111	363.9668
3490.5378	42.6978

2

H	1.092762	1.228480	0.000000
N	0.089455	1.015416	0.000000
N	0.061178	–0.411677	0.592325
N	0.061178	–0.411677	–0.592325

Frequency/ cm^{-1}	Intensity/ $km\ mol^{-1}$
591.7491	5.3959
741.7536	9.7867
1036.9203	48.3882
1454.9633	24.0416
1840.1905	12.8535
3363.6362	4.6772

Table S6. Cartesian coordinates (distances in Å), vibrational frequencies (cm^{-1}), and intensity (km mol^{-1}) for selected structures of HP_3.

HP_3

3

H	1.548561	1.394280	0.000000
P	1.326634	–0.018772	0.000000
P	–0.688510	–0.013298	–1.007755
P	–0.688510	–0.013298	1.007755

Frequency/ cm^{-1}	Intensity/ km mol^{-1}
352.7182	1.0259
438.4073	0.0470
647.9210	1.6027
659.4175	0.6244
846.0875	10.781
2302.280	90.901

4

H	–2.390788	0.584825	0.000000
P	–1.278084	1.478955	0.000000
P	0.000000	–0.129666	0.000000
P	1.437469	–1.388278	0.000000

Frequency/ cm^{-1}	Intensity/ km mol^{-1}
111.3341	0.2016
163.2833	3.0795
441.1667	5.2389
739.7454	11.1728
816.7454	42.3138
2341.602	22.9132

Table S7. Cartesian coordinates (distances in Å), vibrational frequencies (cm^{-1}), and intensity (km mol^{-1}) for selected structures of H_3P_3.

P_3H_3

Anti-5

P	0.029233	–0.645397	1.127027
P	0.029233	1.283946	0.000000
P	0.029233	–0.645397	–1.127027
H	–1.382451	–0.640125	1.300548
H	–1.382451	–0.640125	–1.300548
H	1.449430	1.382977	0.000000
P	0.029233	–0.645397	1.127027

Frequency / cm^{-1}	Intensity/ km mol^{-1}
377.1537	0.9247
382.8298	0.8208
514.9939	0.1269
563.9186	0.0760
602.1165	0.1955
742.1557	10.3672
780.5218	13.0985
872.0006	2.5344
893.3449	0.1125
2358.9785	8.4299
2360.5053	7.0600
2378.4195	111.2949

Syn-5

P	0.000000	1.300921	–0.087978
P	1.126631	–0.650461	–0.087978
P	–1.126631	–0.650461	–0.087978
H	0.000000	1.493424	1.319664
H	–1.293343	–0.746712	1.319664
H	1.293343	–0.746712	1.319664
P	0.000000	1.300921	–0.087978

Frequency/ cm^{-1}	Intensity/ km mol^{-1}
367.3314	0.9835
367.3314	0.9828
508.5089	1.2316
579.7899	0.3307
579.7899	0.3308
676.4354	0.0000
758.9143	12.4858
824.0538	17.6080
824.0538	17.6083
2369.1208	6.0461
2369.1208	6.0461
2392.5988	104.7520

Anti-6

P	1.770623	–0.365611	0.332346
P	–1.392168	–0.172819	–0.678705
P	–0.216194	0.512268	0.839642
H	–2.579937	0.366502	–0.097572
H	1.721980	–0.286803	–1.084177
H	2.491523	0.846221	0.500628

Frequency / cm^{-1}	Intensity/ km mol^{-1}
120.1302	3.3245
171.5776	1.2667
401.5765	7.7005

Syn-6

P	1.567301	–0.220368	0.081888
P	–1.751680	–0.418253	0.033474
P	–0.166724	0.963745	–0.207387
H	–0.995515	–1.626740	0.073015
H	2.646518	0.546734	0.560996
H	1.447676	–1.347583	0.918695

Frequency/ cm^{-1}	Intensity/ km mol^{-1}
156.3681	1.5268
216.9656	16.4374
252.9014	28.4172

486.0301	1.3389	416.9159	2.8832
604.9088	2.4479	476.0025	20.5109
698.7610	11.3783	509.6639	22.3901
727.5308	1.7676	637.3197	3.7773
843.7643	7.9973	782.2949	9.7745
1092.8383	30.5641	1054.2419	47.7889
2337.7706	52.4263	2360.2894	12.7855
2378.5271	37.9351	2435.1554	8.2749
2393.8264	30.0546	2482.9007	6.0420

Table S8. Cartesian coordinates (distances in Å), vibrational frequencies (cm^{-1}), and intensity ($km\ mol^{-1}$) for transition state (TS) structures of P_3H_3.

P_3H_3 – TS

TS-1

P	0.095647	1.036239	0.000000
P	0.095647	–0.503227	1.322928
P	0.095647	–0.503227	–1.322928
H	–0.569049	2.290612	0.000000
H	–1.867527	–1.368690	–0.387970
H	–1.867527	–1.368690	0.387970
P	0.095647	1.036239	0.000000

ν_i = 269.4 cm^{-1}

TS-2

P	–1.330518	–0.570252	–0.122188
P	1.473933	–0.500575	0.107292
P	0.045342	1.019817	–0.024527
H	2.466672	0.203868	–0.647766
H	–2.536876	0.176562	1.004136
H	–2.761156	0.384731	0.234985
P	–1.330518	–0.570252	–0.122188

ν_i = 719.5 cm^{-1}

TS-3

P	–1.663973	0.329975	–0.098515
P	1.722688	0.311523	–0.029106
P	0.090040	–0.819342	0.036622
H	0.531070	1.898940	0.394086
H	–2.512797	–0.506211	0.688585
H	–0.286432	1.898306	0.409093

ν_i = 452.6 cm^{-1}

TS-4

P	0.059809	1.093478	–0.000000
P	0.059809	–0.561182	1.276468
P	0.059809	–0.561182	–1.276468
H	1.162367	1.969053	–0.000000
H	–1.926897	–0.767884	–0.404099
H	–1.926897	–0.767884	0.404099

ν_i = 734.8 cm^{-1}

TS-5

P	–1.597842	–0.592962	0.000000
P	1.825104	–0.293304	0.000000
P	0.000000	0.695467	0.000000
H	2.493544	0.966105	0.000000
H	–2.951236	0.947937	0.386344
H	–2.951236	0.947937	–0.386344

ν_i = 511.5 cm^{-1}

REFERENCES

(1) Turner, A. M.; Kaiser, R. I. Exploiting Photoionization Reflectron Time-of-light Mass Spectrometry to Explore Molecular Mass Growth Processes to Complex Organic Molecules in Interstellar and Solar System Ice Analogs. *Acc. Chem. Res.* **2020**, *53* (12), 2791−2805.

(2) Abplanalp, M. J.; Förstel, M.; Kaiser, R. I. Exploiting Single Photon Vacuum Ultraviolet Photoionization to Unravel the Synthesis of Complex Organic Molecules in Interstellar Ices. *Chem. Phys. Lett.* **2016**, *644*, 79−98.

(3) Frisch, M. J.; Trucks, G. W.; Schlegel, H. B.; Scuseria, G. E.; Robb, M. A.; Cheeseman, J. R.; Scalmani, G.; Barone, V.; Petersson, G. A.; Nakatsuji, H.; Li, X.; Caricato, M.; Marenich, A. V.; Bloino, J.; Janesko, B. G.; Gomperts, R.; Mennucci, B.; Hratchian, H. P.; Ortiz, J. V.; Izmaylov, A. F.; Sonnenberg, J. L.; Williams; Ding, F.; Lipparini, F.; Egidi, F.; Goings, J.; Peng, B.; Petrone, A.; Henderson, T.; Ranasinghe, D.; Zakrzewski, V. G.; Gao, J.; Rega, N.; Zheng, G.; Liang, W.; Hada, M.; Ehara, M.; Toyota, K.; Fukuda, R.; Hasegawa, J.; Ishida, M.; Nakajima, T.; Honda, Y.; Kitao, O.; Nakai, H.; Vreven, T.; Throssell, K.; Montgomery Jr., J. A.; Peralta, J. E.; Ogliaro, F.; Bearpark, M. J.; Heyd, J. J.; Brothers, E. N.; Kudin, K. N.; Staroverov, V. N.; Keith, T. A.; Kobayashi, R.; Normand, J.; Raghavachari, K.; Rendell, A. P.; Burant, J. C.; Iyengar, S. S.; Tomasi, J.; Cossi, M.; Millam, J. M.; Klene, M.; Adamo, C.; Cammi, R.; Ochterski, J. W.; Martin, R. L.; Morokuma, K.; Farkas, O.; Foresman, J. B.; Fox, D. J. *Gaussian 16 Rev. C.01* **2016**.

(4) Becke, A. D. Density-functional Exchange-energy Approximation with Correct Asymptotic Behavior. *Phys. Rev. A* **1988**, *38* (6), 3098−3100.

(5) Lee, C.; Yang, W.; Parr, R. G. Development of the Colle-Salvetti Correlation-energy Formula into a Functional of the Electron Density. *Phys. Rev. B* **1988**, *37* (2), 785−789.

(6) Becke, A. D. Density-functional Thermochemistry. III. The Role of Exact Exchange. *J. Chem. Phys.* **1993**, *98* (7), 5648−5652.

(7) Dunning, T. H. Gaussian Basis Sets for Use in Correlated Molecular Calculations. I. The Atoms Boron Through Neon and Hydrogen. *J. Chem. Phys.* **1989**, *90* (2), 1007−1023.

(8) Bartlett, R. J.; Watts, J. D.; Kucharski, S. A.; Noga, J. Non-iterative Fifth-order Triple and Quadruple Excitation Energy Corrections in Correlated Methods. *Chem. Phys. Lett.* **1990**, *165* (6), 513−522.

(9) Čížek, J. On the Correlation Problem in Atomic and Molecular Systems. Calculation of Wavefunction Components in Ursell-type Expansion Using Quantum-field Theoretical Methods. *J. Chem. Phys.* **1966**, *45* (11), 4256−4266.

(10) Raghavachari, K. Electron Correlation Techniques in Quantum Chemistry: Recent Advances. *Annu. Rev. Phys. Chem.* **1991**, *42* (1), 615−642.

(11) Stanton, J. F. Why CCSD(T) Works: A Different Perspective. *Chem. Phys. Lett.* **1997**, *281* (1), 130−134.

(12) Peterson, K. A.; Woon, D. E.; Dunning, T. H. Benchmark Calculations with Correlated Molecular Wave Functions. IV. The Classical Barrier Height of the $H+H_2 \rightarrow H_2+H$ Reaction. *J. Chem. Phys.* **1994**, *100* (10), 7410−7415.